Reaction Dynamics

Dynamic Effects on [3,3] and [1,3] Shifts of 6-Methylenebicyclo[3.2.0]hept-2-ene**

Christopher P. Suhrada, Cenk Selçuki, Maja Nendel, Carina Cannizzaro, K. N. Houk, Peter-Jürgen Rissing, Dirk Baumann, and Dieter Hasselmann**

Dedicated to Professor Wolfgang Kirmse on the occasion of his 75th birthday

The controversies over concerted versus stepwise diradical mechanisms of potentially pericyclic reactions have subsided with improvements in the understanding of stereoselectivity in thermal rearrangements that involve modestly stabilized diradical intermediates. The thermal rearrangements of vinylcyclopropanes[1] and vinylcyclobutanes,[2] including bicyclo[3.2.0]hept-2-ene,[3] involve diradical intermediates that lack a deep potential energy well, and their outcomes deviate from statistical predictions. The thermal rearrangement of 6-methylenebicyclo[3.2.0]hept-2-ene (**1**) to 5-methylenenorbornene (**3**) is more intriguing, as it yields a nonrandom distribution of products despite the stabilizing effect of the 6-methylene substituent on the intermediate **2**.

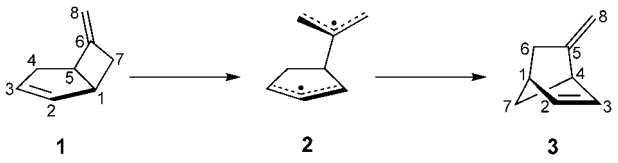

Dideuterio labeling has revealed a preference for [1,3] over [3,3] shifts,[4] and the stereochemistry observed with methyl labels has led to the hypothesis that diradical intermediates do not equilibrate rotationally before collapsing to form the bicyclic products.[5] New experimental studies of monodeuterated species currently show modest levels of both regio- and stereoselectivity (Table 1),[6] and DFT and ab initio calculations provide a theoretical framework for understanding these results.

Table 1: Deuterium label distribution in product **3** from the thermolysis of 7*x*-, 8*E*-, and 8*Z*-**1**, extrapolated to $t = 0$ min.

Educt	6*x*-**3**	6*n*-**3**	8*E*-**3**	8*Z*-**3**
7*x*-**1**	0.37	0.20	0.22	0.21
8*E*-**1**	0.13	0.23	0.64	–
8*Z*-**1**	0.24	0.14	–	0.62

UB3LYP and CASSCF calculations indicate that two modes of C1–C7 cleavage produce stereoisomeric diallyl intermediates **2** from **1** (Figure 1). The favored transition state, **TS-12n**, moves C7 toward C3 and places the 7*x* substituent in an *E* configuration. In contrast, **TS-12x** moves C7 away from C3 and puts the 7*x* substituent in the *Z* position. The preference (1.8 kcal mol^{-1}; CASPT2//UB3LYP) for **TS-12n** over **TS-12x** is analogous to torquoselectivity in electro-

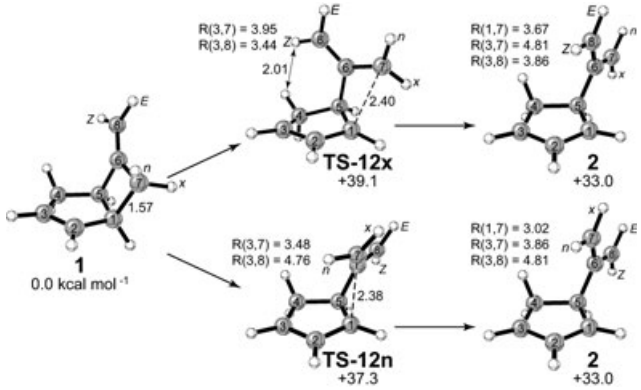

Figure 1. Two transition states for bond breaking lead to stereoisomeric diallyl intermediates **2**. Structures shown are (U)B3LYP-optimized with selected bond distances indicated in angstroms. Enthalpy values (CASPT2//UB3LYP), in kcal mol^{-1} relative to that of **1**, are listed below each structure label.

[*] C. P. Suhrada, Dr. C. Selçuki, Dr. M. Nendel, Dr. C. Cannizzaro, Prof. Dr. K. N. Houk
Department of Chemistry and Biochemistry
University of California, Los Angeles
Los Angeles, CA 90095-0569 (USA)
Fax: (+1) 310-206-8143
E-mail: houk@chem.ucla.edu
Dr. P.-J. Rissing, Dr. D. Baumann, Prof. Dr. D. Hasselmann
Fakultät für Chemie, Organische Chemie II
Ruhr-Universität Bochum
44780 Bochum (Germany)
Fax: (+49) 234-32-14109
E-mail: dieter.hasselmann@ruhr-uni-bochum.de

[**] Work at UCLA was supported by the National Science Foundation (research grant to K.N.H. and IGERT fellowship to C.P.S.) and TUBITAK (fellowship to C.S.). The Bochum group thanks the Deutsche Forschungsgemeinschaft and Fonds der Chemischen Industrie.

Supporting information for this article is available on the WWW under http://www.angewandte.org or from the author.

  DOI: 10.1002/ange.200500027

cyclic ring openings;[7] the favored structure minimizes closed-shell repulsion and maximizes hyperconjugation between the orbitals of the breaking C1–C7 σ bond and the C2–C3 π bond. Also, **TS-12x** brings the 8*Z* hydrogen atom into close proximity with the one in the 4-*cis* position.

The diradical **2** lies 4.3 kcal mol^{-1} below **TS-12n**. Once formed, **2** can isomerize by rotation about the C5–C6 bond with a calculated barrier of only 2.4 kcal mol^{-1} (**TS-22**, Figure 2). This motion exchanges the positions of C7 and C8. Allylic stabilization preserves the pseudo-*E*/*Z* configuration of C7 and C8 substituents during the lifetime of the intermediate; barriers for rotation about C6–C7 and C6–C8 are calculated to be ≈12–13 kcal mol^{-1} higher than those that separate **2** from the product **3**.

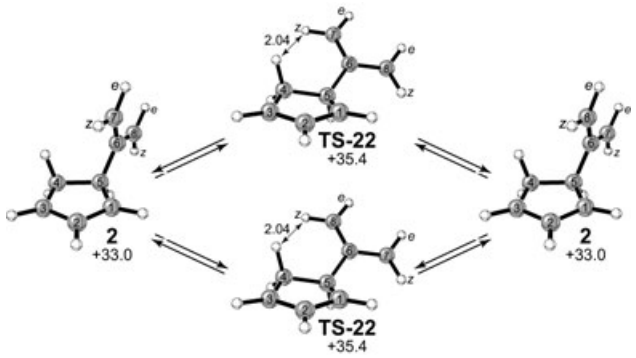

Figure 2. Rotation about C5–C6 exchanges the position of proximal and distal allyl termini, yet the pseudo-*E*/*Z* configuration of substituents is preserved. Structures shown are (U)B3LYP-optimized with selected bond distances indicated in angstroms. Enthalpy values (CASPT2//UB3LYP), in kcal mol^{-1} relative to that of **1**, are listed below each structure label.

In analogy to the bond-breaking step, the formation of a new bond at C3 can occur in two different stereochemical senses (Figure 3). Both transition states involve the formation of a bond between C3 and the proximal allyl terminus in **2**.[8] From a given intermediate **2**, the two products **3** that can be formed are thus epimers with respect to the substituents on that carbon. **TS-23n** is favored slightly and places the pseudo-*E* substituent in the 6*x* position in the product; **TS-23x** places the same substituent in the 6*n* position.

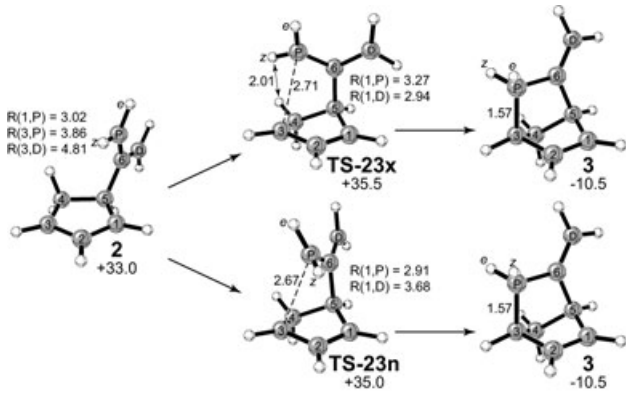

Figure 3. Two cyclization routes form epimeric products from a given intermediate **2**. Structures shown are (U)B3LYP-optimized with selected bond distances indicated in angstroms. Enthalpy values (CASPT2//UB3LYP), in kcal mol^{-1} relative to that of **1**, are listed below each structure label.

TS-23n and **TS-23x** lie only 2.0 and 2.5 kcal mol^{-1} above **2**, respectively. Compared with 2.4 kcal mol^{-1} for **TS-22**, this suggests that cyclization competes with conformational isomerization in the intermediate, and therefore a majority of products will come from an intermediate in the conformation in which it is initially formed.

These pathways imply the kinetic model outlined in Scheme 1 for a single-labeled system. For comparison with the experimental zero-time data, reversions from **2** to **1** may

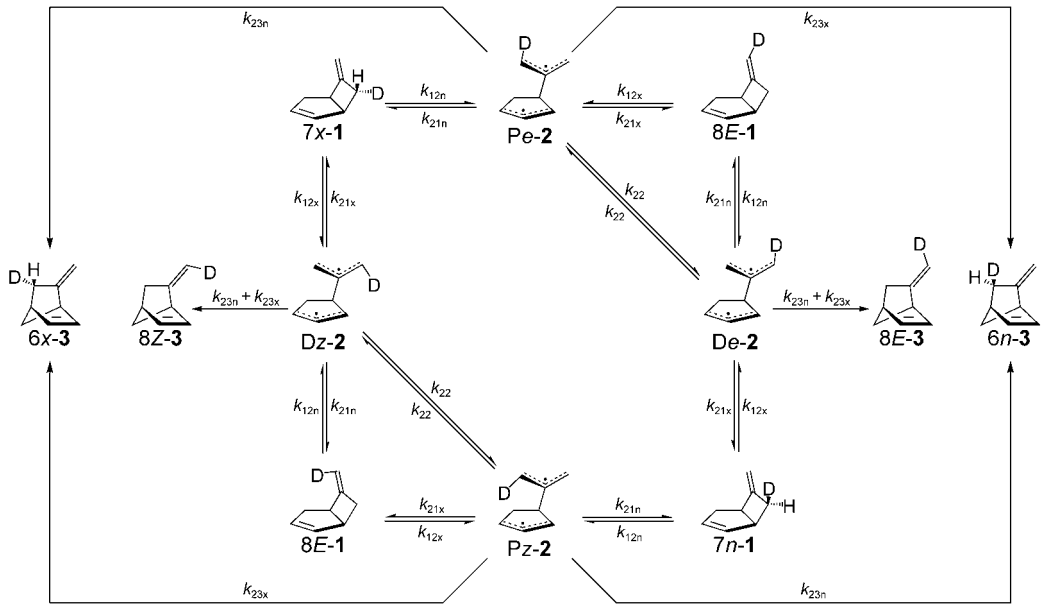

Scheme 1. Stepwise kinetic model for rearrangements of **1** bearing a single deuterium label on C7 or C8.

be ignored,[9] and the relative yield of products can be computed based on three independent parameters, related to k_{12n} versus k_{12x}, and k_{23n} versus k_{23x} versus k_{22} (Supporting Information).

With the model in Scheme 1 and the selectivity parameters from CASPT2//UB3LYP transition-state energies, calculations predict the product distribution listed in Table 2, Column 2. The major products of both experiments are correctly identified, although the minor product ratios deviate from experiment markedly.

Table 2: Product distributions from experiment, CASPT2//UB3LYP calculations, and least-squares fits of two theoretical models to the experimental data. Corresponding kinetic parameters and relative TS energies are listed along with predicted product distributions.[a]

	Experiment	CASPT2//UB3LYP (fully stepwise)	Least-squares fit (fully stepwise)	Least-squares fit (stepwise plus concerted [3s,3s])
7*x*-**1**→6*x*-**3**	0.37	0.39	0.33	0.39
7*x*-**1**→6*n*-**3**	0.20	0.25	0.28	0.22
7*x*-**1**→8*E*-**3**	0.22	0.26	0.20	0.20
7*x*-**1**→8*Z*-**3**	0.21	0.10	0.19	0.19
8*E*-**1**→8*E*-**3**[b]	0.63	0.64	0.62	0.61
8*E*-**1**→6*n*-**3**[b]	0.23	0.13	0.17	0.24
8*E*-**1**→6*x*-**3**[b]	0.14	0.23	0.21	0.15
R^2[c]	(1.000)	(0.251)	0.628	0.969
$k_{12n}/(k_{12n}+k_{12x})$	–	0.861	0.744	0.797
$k_{22}/(2k_{22}+k_{23n}+k_{23x})$	–	0.308	0.265	0.252
$k_{23n}/(k_{23n}+k_{23x})$	–	0.634	0.556	0.643
Fraction direct **TS-12x** to [3*s*,3*s*]-**3**	–	–	–	0.808
$\Delta\Delta G^{\ddagger}_{(\text{TS-12x}-\text{TS-12n})}$	–	+1.8	+1.0	+1.3
$\Delta\Delta G^{\ddagger}_{(\text{TS-22}-\text{TS-23n})}$	–	+0.4	+0.7	+0.9
$\Delta\Delta G^{\ddagger}_{(\text{TS-23x}-\text{TS-23n})}$	–	+0.5	+0.2	+0.6

[a] For CASPT2//UB3LYP, relative TS energies ($\Delta\Delta H^{\ddagger}$) give parameters that produce the product distribution. Least-squares fits produce both kinetic parameters and expected values for the product distribution; relative TS energies are calculated from the kinetic parameters thus obtained. [b] The 8*E*-**1** and 8*Z*-**1** experiments are redundant under all models considered, excluding isotope effects. For this reason, they have been averaged for comparison and fit to theory to simplify the analysis and not to assign the two 8-*d*-**1** experiments undue weight in comparison with the single 7-*d*-**1** experiment. For example, the entry for 8*E*-**1**→6*n*-**3** is actually the average of experimental proportion in which 8*E*-**1** forms 6*n*-**3**, and 8*Z*-**1** forms 6*x*-**3**. [c] $R^2=\Sigma(\gamma_{\text{predicted}}-\gamma_{\text{expt}})^2/\Sigma(\gamma_{\text{expt}}-\gamma_{\text{random}})^2$ in which γ_{random} represents the hypothetical nonselective product distribution: $\gamma_{\text{random}}=0.25$ for each product except the [1,3] product in the 8-*d*-**1** experiment, for which $\gamma_{\text{random}}=0.50$. Although the CASPT2//UB3LYP prediction does not involve a fit to experiment, the R^2 analysis is applied for comparison with the least-squares results.

We have also worked backward from the experimental result by means of a least-squares fit, to determine what combination of relative rates would lead to the observed outcome. Such a fit produces selectivity parameters and a corresponding expected product distribution, shown in Column 3 of Table 2. The fit parameters match the experimental outcome more closely, despite the fact that they differ only slightly from the CASPT2//UB3LYP predictions. However, closer inspection shows that the fit still does not reproduce the experimental result satisfactorily in all cases. For instance, the ratio among [3,3] products from 8-*d*-**1** (i.e., 8*E*-**1** and 8*Z*-**1**) is reversed, whereas the proportion of [1*r*,3*s*] products in the 7*x*-**1** experiment is higher than it should be.

The problem is solved by incorporating a concerted Cope pathway into the stepwise model. The addition of a corresponding fourth selectivity parameter, described below, improves the fit from $R^2=0.628$ to $R^2=0.969$ (Table 2, Column 4). The goodness of fit alone is evidence to support the presence of such a pathway, yet how can this be reconciled theoretically? Examination of the potential energy surface of the reaction gives clues to what may be happening.[10] Preliminary single-point energy calculations prompted us to suspect that a CASPT2//UB3LYP treatment[11] would give the most accurate representation of the PES shape (Figure 4a). At this level of theory, the **TS-12x** saddle point lies at a low value of R(3,8), and the transition vector has a component in the negative R(3,8) direction. At the same time, the flattening of the diradical potential energy well shifts **TS-23x** toward larger values of R(3,8), positioning it almost directly in front of **TS-12x**. Thus situated, one can easily envision how **TS-23x** might bifurcate the ensemble of trajectories passing over **TS-12x**, sending them either to intermediate **2** or to the product **3** (Figure 4b).[12]

According to this model, **TS-12x** is populated based on its relative free energy, as before. After the transition state, that population is divided into two portions according to a new parameter. One portion goes to **2** and a statistical distribution of products from there, and the other produces [3*s*,3*s*]-**3** directly. The relative TS energies corresponding to this fit are listed in Table 2 and agree reasonably well with CASPT2//UB3LYP values. As for the additional parameter, the fit suggests that $81\pm16\%$ of the **TS-12x** trajectories (16% of the total product distribution) go directly to **3**.

Having obtained an adequate quantitative fit between theory and experiment, we consider the fact that the experimental [1,3]/[3,3] ratio is subject to a large positional secondary isotope effect, outside of probable error limits: [1,3]/[3,3] = 58:42 from 7*x*-**1** but 63:37 from 8*E*-**1** or 8*Z*-**1** (see also Reference [4]). This remains puzzling: although our calculations predict reasonable isotope effects for the various rate constants in Scheme 1, their combined effect (60:40 from 7*x*-**1** versus 61:39 from 8-*d*-**1**) is much smaller than what is experimentally observed.

In summary, experiments and calculations reported herein establish how [1,3] versus [3,3] and [1*i*,3*s*] versus [1*r*,3*s*] preferences may arise in a strictly stepwise reaction as a result of stereoelectronic effects on the breakage and formation of bonds, along with incomplete conformational equilibration among intermediate diradicals. Whereas much of the observed selectivity can be explained by a fully stepwise, statistical model, we find that there is also a role for a formally concerted Cope pathway in the form of a nonstatistical post-

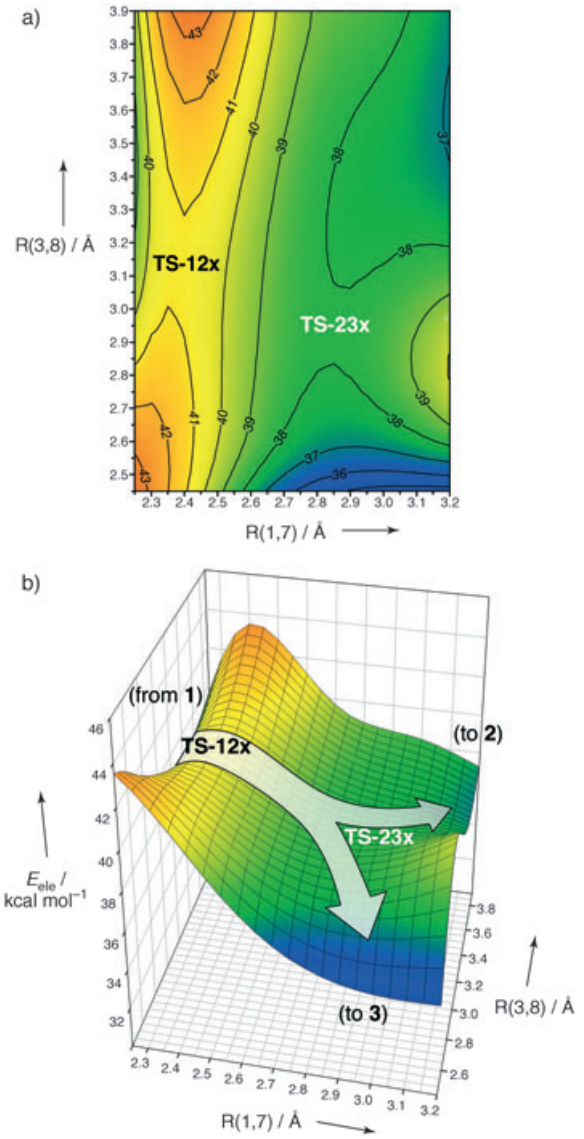

Figure 4. a) Two-dimensional projection of the potential energy surface for the rearrangement of **1** to **3**. The plot was mapped with CASPT2 single-point energy calculations on UB3LYP constrained-optimized structures at intervals of 0.05 Å in the coordinates R(1,7) and R(3,8), the bond-breakage and formation distances, respectively, for a [3,3] shift. Energy contours are marked in kcal mol^{-1}, relative to **1**. b) Three-dimensional representation of plot in part a) that schematically illustrates the concept of bifurcation of **TS-12x** reaction trajectories by **TS-23x**.

transition-state bifurcation. Dynamic simulations may yield additional insight into this process.

Experimental Section

The preparation of 7*x*-, 8*E*-, and 8*Z*-**1** is described in the Supporting Information. Thermolyses were carried out in the gas phase at 220 °C in a 20-L reaction flask at 1 to 3 mbar. *n*-Nonane served as an internal standard and *n*-hexane as collision partner. Samples were taken after approximately 20 %, 40 %, 60 %, and 80 % structural isomerization of starting material. Besides **3**, the only products observed were isotopomers of **1**. Ratios of individual isotopomers were determined by ^{2}H NMR spectroscopy (61.4 MHz) after separation of structural isomers by vapor-phase gas chromatography. Isotopomeric ratios were extrapolated to a thermolysis time $t = 0$ (Table 1).

Structures of **1** and **3**, as well as that of the intervening diradical **2** and associated transition species were optimized with both UB3LYP/6-31G(d) and (6,6)CASSCF/6-31G(d) in Gaussian 98.[13] (6,6)CASPT2/6-31G(d) single-point energies were calculated for both sets of stationary points in MOLCAS.[14] Kinetic isotope effects were calculated in the program Quiver[15] based on UB3LYP/6-31G(d) frequency data.

Received: January 4, 2005
Published online: April 28, 2005

Keywords: ab initio calculations · density functional calculations · diastereoselectivity · reaction mechanisms · sigmatropic rearrangement

[1] a) K. N. Houk, M. Nendel, O. Wiest, J. W. Storer, *J. Am. Chem. Soc.* **1997**, *119*, 10545; b) C. Doubleday, M. Nendel, K. N. Houk, D. Thweatt, M. Page, *J. Am. Chem. Soc.* **1999**, *121*, 4720; c) M. Nendel, D. Sperling, O. Wiest, K. N. Houk, *J. Org. Chem.* **2000**, *65*, 3259; d) C. Doubleday, *J. Phys. Chem. A* **2001**, *105*, 6333.
[2] P. A. Leber, J. E. Baldwin, *Acc. Chem. Res.* **2002**, *35*, 279.
[3] a) J. A. Berson, G. L. Nelson, *J. Am. Chem. Soc.* **1967**, *89*, 5503; b) J. A. Berson, G. L. Nelson, *J. Am. Chem. Soc.* **1970**, *92*, 1096; c) J. E. Baldwin, K. D. Belfield, *J. Am. Chem. Soc.* **1988**, *110*, 296; d) F.-G. Klärner, R. Drewes, D. Hasselmann, *J. Am. Chem. Soc.* **1988**, *110*, 297; e) B. K. Carpenter, *J. Am. Chem. Soc.* **1995**, *117*, 6336; f) B. K. Carpenter, *J. Am. Chem. Soc.* **1996**, *118*, 10329.
[4] a) D. Hasselmann, *Tetrahedron Lett.* **1972**, *13*, 3465; b) D. Hasselmann, *Tetrahedron Lett.* **1973**, *14*, 3739.
[5] D. Hasselmann, *Angew. Chem.* **1975**, *87*, 252; *Angew. Chem. Int. Ed. Engl.* **1975**, *14*, 257.
[6] a) P.-J. Rissing, PhD Dissertation, Ruhr University, Bochum (Germany), **1978**; b) D. Baumann, PhD Dissertation, Ruhr University, Bochum (Germany), **2001**.
[7] W. R. Dolbier, Jr., H. Koroniak, K. N. Houk, C. Sheu, *Acc. Chem. Res.* **1996**, *29*, 471.
[8] It is immediately evident that **TS-23n** forms a bond from C3 to the *proximal* allyl terminus. Although it appears feasible that **TS-23x** might involve rotation of the *distal* allyl carbon past C4 and into bonding distance with C3, IRC calculations show that this is not the case: the bond is formed to the proximal carbon in **TS-23x** as well as **TS-23n**.
[9] Although isotopomers of the educt **1** begin to accumulate with time, their effect on the distribution of labels in the product **3** vanishes upon extrapolation to $t = 0$. Examination of **1** at high levels of conversion shows a preponderance of the starting isotopomer, indicating that educt isomerization is slow in comparison with product formation. Regardless of its magnitude, the rate k_{21} is the same for all intermediates **2**, and therefore may be ignored in the computation of label distribution in product **3**.
[10] A transition state for a concerted [3*s*,3*s*] reaction, as well as one for a concerted [1*i*,3*s*] process, can be located with RB3LYP/6-31G(d) (Supporting Information), but these saddle points are only artifacts of the restricted formalism, and they disappear at the UB3LYP level.
[11] A CASPT2 single-point energy calculation was performed on each of the UB3LYP constrained-optimized structures used to construct the UB3LYP surface.
[12] A PES involving a post-TS bifurcation between a Cope pathway and formation of an allylic-stabilized diradical intermediate has been discussed in the case of an acyclic allenic triene: S. L.

Debbert, B. K. Carpenter, D. A. Hrovat, W. T. Borden, *J. Am. Chem. Soc.* **2002**, *124*, 7896.
[13] Gaussian 98 (Revision A.9), M. J. Frisch, G. W. Trucks, H. B. Schlegel, G. E. Scuseria, M. A. Robb, J. R. Cheeseman, V. G. Zakrzewski, J. A. Montgomery, R. E. Stratmann, J. C. Burant, S. Dapprich, J. M. Millam, A. D. Daniels, K. N. Kudin, M. C. Strain, O. Farkas, J. Tomasi, V. Barone, M. Cossi, R. Cammi, B. Mennucci, C. Pomelli, C. Adamo, S. Clifford, J. Ochterski, G. A. Petersson, P. Y. Ayala, Q. Cui, K. Morokuma, D. K. Malick, A. D. Rabuck, K. Raghavachari, J. B. Foresman, J. Cioslowski, J. V. Ortiz, B. B. Stefanov, G. Liu, A. Liashenko, P. Piskorz, I. Komaromi, R. Gomperts, R. L. Martin, D. J. Fox, T. Keith, M. A. Al-Laham, C. Y. Peng, A. Nanayakkara, M. Challacombe, P. M. W. Gill, B. G. Johnson, W. Chen, M. W. Wong, J. L. Andres, C. Gonzalez, M. Head-Gordon, E. S. Replogle, J. A. Pople, Gaussian, Inc., Pittsburgh, PA, **1998**.
[14] MOLCAS (Version 5.0), K. Andersson, M. Barysz, A. Bernhardsson, M. R. A. Blomberg, D. L. Cooper, T. Fleig, M. P. Fülscher, C. de Graaf, B. A. Hess, G. Karlström, R. Lindh, P.-Å. Malmqvist, P. Neogrády, J. Olsen, B. O. Roos, A. J. Sadlej, B. Schimmelpfennig, M. Schütz, L. Seijo, L. Serrano-Andrés, P. E. M. Siegbahn, J. Stålring, T. Thorsteinsson, V. Veryazov, P.-O. Widmark, Lund University, Sweden, **2001**.
[15] M. Saunders, K. E. Laidig, M. Wolfsberg, *J. Am. Chem. Soc.* **1989**, *111*, 8989.

